Publisher: Taylor & Francis
Journal: *Journal of Coordination Chemistry*
DOI: http://dx.doi.org/10.1080/00958972.2016.1167885

Pharmacological activities of a propylthiouracil compound structurally modified by coordination with copper(II)

NORA M. URQUIZA[a], LUCIANA G. NASO[b], JUAN J. MARTÍNEZ MEDINA[b,d], MARÍA A. MOYANO[a], LUIS LEZAMA[c], PATRICIA A. M. WILLIAMS[b] and EVELINA G. FERRER*[b]

[a]Cátedra de Química Analítica, Instituto de Química Analítica, Facultad de Bioquímica, Química y Farmacia, Universidad Nacional de Tucumán, Ayacucho 471, 4000 San Miguel de Tucumán, Argentina
[b]Centro de Química Inorgánica (CEQUINOR/CONICET, UNLP), Facultad de Ciencias Exactas, UNLP, C. Correo 962, 1900 La Plata, Argentina
[c]Departamento de Química Inorgánica, Facultad de Ciencia y Tecnología, Universidad del País Vasco UPV/EHU, P.O. Box 644, 48080 Bilbao, Spain and BCMaterials, Parque Científico y Tecnológico de Bizkaia, Edificio 500-1, 48160 Derio, Spain
[d]Departamento de Química, UNCAUS, Cte. Fernández 755 (3700), Chaco, Argentina

Abbreviations

CFU	Colony forming units
NADH	NADH Reduced nicotinamide adenine dinucleotide

Abstract

For the first time, pharmacological activities for propylthiouracil (actually used as antithyroid drug) were determined. In addition, a new propylthiouracil copper(II) complex ($[Cu(PTU)_2]_2$) was synthesized and characterized by FTIR, EPR, UV-visible and diffuse reflectance spectroscopies including elemental analysis, dissolution profiles and stability studies. Taking into account the correlation between Graves' disease and the formation of reactive oxygen species (ROS) and other free radicals, the ligand and the complex were tested for their antioxidant effects on $O_2^{\bullet-}$ and $OH^{\bullet}$ radicals. A significant increase in the disruption of $OH^{\bullet}$ radical was observed for PTU and its copper(II) complex, but neither of them have the ability to dismutate the $O_2^{\bullet-}$ radical. Antimicrobial activities were also determined observing that the complex is very active against Gram-positive bacteria. In addition, the ability of PTU and its complex to inhibit acid and alkaline phosphatases were analyzed. Results showed that PTU had no effect while the complex behaved as a potent ALP (alkaline phosphatases) inhibitor. Finally, albumin interaction experiments denoted high affinity

*Corresponding author. Email: evelina@quimica.unlp.edu.ar

towards the complex in contrast with PTU with a constant binding value two hundred times higher than the ligand and bearing two binding sites. Based on this study, it has been hypothesized that $([Cu(PTU)_2]_2$ would be a promising candidate for further evaluation as an antioxidant, antimicrobial and phosphatase alkaline inhibitor agent.

Keywords: Antimicrobial activity; Antioxidants; BSA Interactions; Copper(II); Propylthiouracil

1. Introduction

Antithyroid drugs (methimazole, propylthiouracil (6-*n*-propyl-2-thiouracil), 6-methyl-2-thiouracil, carbimazole, *etc*.) are well known and their effectiveness proved and compared [1-3]. Many studies, including selenium analogue products, have been tested as antithyroid drugs [4, 5]. Nevertheless, these typical drugs have not been exhaustively tested on other pathologies. There is some evidence about the potential of methimazole inhibiting prostaglandin H synthase-catalyzed xenobiotic oxidation by inhibiting the formation of a hydroperoxide (*i.e*. prostaglandin G_2). Oxidation of xenobiotics by peroxidases has been proposed as an activation mechanism of chemical carcinogens, particularly in extrahepatic tissues. Its action mechanism has been suggested that methimazole reduces free radicals, thus inhibiting accumulation of these oxidation products and consequently their interaction with cellular macromolecules to produce toxic and/or carcinogenic sequel [6]. Methimazole has been also proved as an effective depigmenting agent being non-cytotoxic and non-mutagenic [7]. Some of these biological properties were mentioned in our previous work when we began to investigate the formation and pharmacological properties of copper(II) coordination complexes using methimazole as ligand [8-10]. A series of studies were performed to determine the efficiency of the methimazole and their complexes in inhibiting alkaline (ALP) and acid phosphatase (AcP), and antioxidant and antibacterial activities and interaction ability with bovine serum albumin (BSA) were also determined. In previous work, we demonstrated the ability of methimazole to inhibit ALP (IC_{50} = 70 μM) having moderate behavior that was improved after complex formation (Cu-Met = $[Cu(Met)_2(H_2O)_2](NO_3)_2{\cdot}H_2O$, Met = methimazole, IC_{50} = 42 μM) [10]. On the contrary, it was not the case for the ternary complex with phenanthroline ($[Cu(Met)_2(phen)(H_2O)_2]Cl_2$, Cu-Met-phen, phen = phenanthroline,) which was 50% less active than Cu-Met at 100 μM concentration [8]. However, when inhibition of AcP was evaluated, the presence of phen was relevant in the specific effect on the enzyme (Cu-Met-phen IC_{50} = 300 μM).

Coordination significantly improves the inhibition behavior in comparison with the effect of Cu-Met (Cu-Met, 22% of inhibition at 500 μM)) and that of the inactive methimazole.

There is a direct relationship between Graves' disease and radicals [11-13]. Alteration in the thyroid function had effect on the respiratory chain compound activities of rat liver mitochondria suggesting that this dysfunction led to accelerated reactive oxygen species formation causing changes in the antioxidant protective system potential. For this reason, we evaluate the antioxidant properties by the determination of the capacity of the tested compound to simulate the activity of the superoxide dismutase (SOD) enzyme. We found that methimazole had no activity and coordination with phen acted in disadvantage (catalytic activity) and only copper(II) methimazole complexation produced a metal-drug synergy behavior with an excellent IC_{50} value of 3.0 μM. Associated with the antimicrobial activities, it was established that the presence of Cu(II) (Cu-Met) and Cu(II) and phen (Cu-Met-phen) remarkably improves the antibacterial activity of methimazole especially on *S. aureus*, *S. epidermidis* and *E. faecalis* from weak to moderate or significant action [8].

In addition, we have found in the literature experiments related to the antiperoxidase activity of propylthiouracil and its metabolites [14] as well as the measurement of the inhibitory effect on type I iodothyronine deiodinase and the antithyroid activity for selenium analogues of propylthiouracil [15]. Literature data also reported the structural analysis of Cu(I) complexes containing PTU [16] and triphenylphosphine (tpp) or tri(p-tolyl)phosphine (tptp), ([$CuI(PTU)_2$](toluene), [$CuI(tpp)_2(PTU)$], [$CuI(tptp)_2(PTU)$]) and of Hg(II) complexes [17] $HgI_2(PTU)_2 \cdot MeOH$], [$HgI_2(PTU)_2 \cdot HgI_2$]), but their biological activities were not determined.

Following our general interest in the biological properties of antithyroid drugs and its metal complexes, we presented in this work new pharmacological activities for propylthiouracil and its compound with copper(II).

2. Experimental

2.1. *Materials and instrumentation*

All chemicals were of analytical grade. Copper(II) nitrate trihydrate was obtained from Merck, propylthiouracil (PTU), para-nitrophenyl phosphate (p-NPP), anhydrous lactose and all the other analytical grade chemicals used were purchased from Sigma. Bovine Serum Albumin BSA (A-6003, essentially fatty acid-free) and acid phosphatase AcP (from potato, 0.8 U/mg,

Deisenhofen, product number P-3752) were obtained from Sigma Chemical Company (St. Louis, MO) and used as supplied.

FTIR spectra of powdered samples were measured with a Bruker IFS 66 FTIR-spectrophotometer from 4000 to 400 cm^{-1} as KBr pellets. Electronic absorption spectra were recorded on a Hewlett-Packard 8453 diode-array spectrophotometer using 1 cm quartz cells. Diffuse reflectance spectra were registered with a Shimadzu UV-300 instrument using MgO as an internal standard. Elemental analyses for carbon, hydrogen and sulfur were performed using a Carlo Erba EA 1108 analyzer. For the dissolution capacity test a Hanson Research SR6 (Apparatus 2-Paddle Apparatus) equipment and a Spectrophotometer Metrolab 1700 were used. To record the EPR spectra of the compounds at different temperatures, a Bruker ESP300 spectrometer operating at X and Q-bands and equipped with standard Oxford low temperature devices was used. The magnetic field was measured with a Bruker BNM 200 gaussmeter, and the frequency inside the cavity was determined by using a Hewlett-Packard 5352B microwave frequency counter. A computer simulation of the EPR spectra was performed using the SimFonia programs (WINEPR SimFonia 1996).

2.2. *Synthesis of $[Cu(PTU)_2]_2$*

A solution was prepared by dissolving 1 mmol of PTU in 10 mL of absolute ethanol under continuous stirring. To this solution, 0.5 mmol of $Cu(NO_3)_2 \cdot 2.5H_2O$ previously dissolved in 3 mL of absolute ethanol was added. The final pH value was 3.5. The solution turned its color from green to violet and finally after 15 min a violet microcrystalline powder precipitate was obtained. The solid was washed several times with absolute ethanol and stored in an oven at 60 °C. Table 1 summarizes the analytical data, the solubility of the complex and the UV-vis and EPR spectral data. Solubility tests showed that the complex was not soluble in water and organic solvents (and mixtures of both) either at room or boiling temperatures. It was only soluble in DMSO and in the conditions of the dissolution profiles studies (see below).

The diagram for synthesis of $[Cu(PTU)_2]_2$ is presented in scheme 1. Copper(II) exhibits a square planar geometry, where two ligands are bidentate bridging coordination (N and S) and the other two ligands also coordinated through N and S (see below).

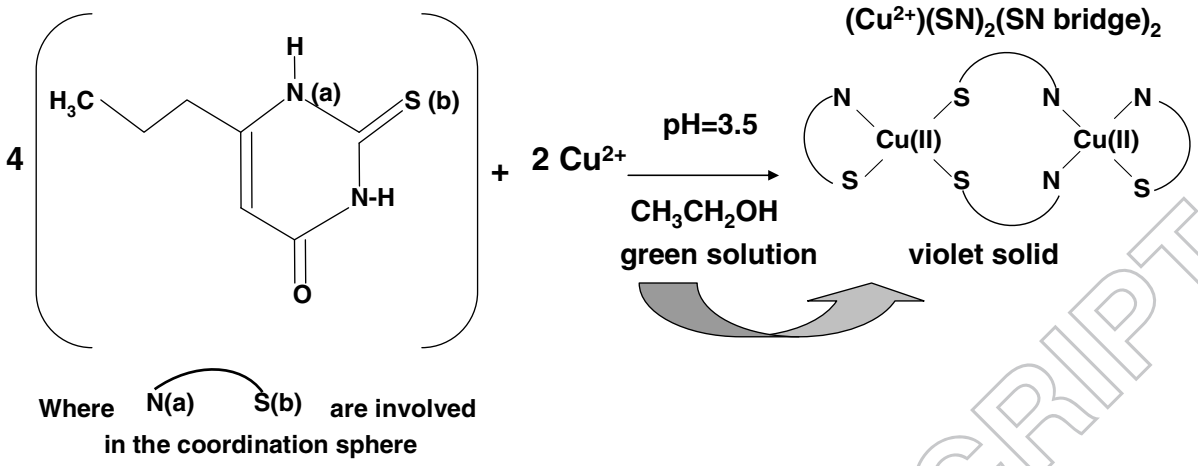

Scheme 1. Schematic diagram for complexation processes.

2.3. *Dissolution profiles of the complexes*

The dissolution profiles were performed according to the United States Pharmacopeia (USP 30). Capsules No. 3 were prepared with homogenous mixture (50 mg of the complex and 130 mg of anhydrous lactose) according to propylthiouracil formulation [18]. Dissolution testing of capsules was performed in distilled water (pH 5–6), HCl 0.1 M, sodium lauryl sulfate (LSNa) 0.01 M and buffer KH_2PO_4 (pH 6.8, 0.2 M) and simulated gastric medium NaCl (2 g/L) and HCl (6.0 mL/L) with a final pH value of 1.2. The final volume of the dissolution medium was 500 mL at 37 °C, and the mixture was stirred at 100 rpm. For dissolution profiles, 10.0 mL aliquots were withdrawn at 5, 10, 20, 30, 40, 50 and 60 min. The solutions were immediately filtered through 0.45 µM nylon filter. 1 mL of the filtered aliquots was pipetted into 25 mL volumetric flask for each compound with fresh dissolution fluids in each case. The percentage of drug release was assayed by electronic spectroscopy and the UV absorbance was measured at 274 nm. Cumulative percentages of the dissolved drug from the tablets were calculated and plotted versus time.

2.4. *Stability studies*

In order to determine the stability of the compounds during the preparation of the solutions for the *in vitro* measurements, the variation of the UV-vis spectra with time was performed. Because of the low solubility of the complexes in water, the dissolution has been carried out in DMSO. The copper(II) d-d electronic absorption bands in the visible spectral range were monitored.

2.5. *Phosphatases inhibition tests*

2.5.1. Alkaline phosphatase specific activity. The effect of the PTU and the $[Cu(PTU)_2]_2$ complex on ALP activity was determined by UV–vis spectroscopy [8]. The reaction was started by addition of the substrate paranitrophenyl phosphate (p-NPP) and the product p-nitrophenol was monitored by absorbance changes at 405 nm. Briefly, the experimental conditions for ALP specific activity measurement were as follows: 1 µg/mL of bovine intestinal ALP and 5 mM of p-NPP were dissolved in the incubation buffer (55 mM glycine + 0.55 mM $MgCl_2$, pH 10.4) and held for 10 min. The effects of the compounds were determined by addition of different concentrations (1-500 µM) of each one to the pre-incubated mixture. The solutions of the complexes were prepared in DMSO before adding the buffer to obtain the desired final concentrations. The effect of each concentration was tested at least in triplicate in three different experiments.

2.5.2. Acid phosphatase inhibition test. Acid phosphatase inhibition test was performed according to Blum and Schwedt procedures [19]. Acetate buffer was prepared by dissolving a volume of 5.72 mL of concentrated acetic acid in distilled water (final volume of 250 mL) adjusting the pH to 5.60 with 0.5 M NaOH. The stock solution of the enzyme was prepared by mixing 12.5 mg of the 0.25 U/mL acid phosphatase powder in 2.0 mL acetate buffer. For the measurements, 100 µL of the stock solution was diluted with 1.9 mL acetate buffer. For the substrate solution 0.170 g of p-NPP was dissolved in 2.5 mL distilled water.

Test procedure: the compound solutions were prepared by diluting the stock solutions prepared in DMSO with acetate buffer. A volume of 0.50 mL of complex solution was mixed with 0.10 mL of the enzyme solution and 1.00 mL of buffer. The mixture was kept at 25 °C for 20 min (incubation time). After starting the reaction by adding 0.10 mL of the substrate solution, the tube was kept at 25 °C for 20 min. The reaction was stopped with the addition of 0.50 mL of a 0.5 M sodium hydroxide solution. The enzymatic activity was finally calculated by measuring the absorbance of 4-nitrophenolate at 405 nm against a blank prepared without the enzyme. Three independent replicates of each point were measured.

In both experiments, 100% of the enzyme activity is assigned to a basal measurement containing all the reaction media including the same volume of DMSO in all the tests. It is worthy to mention that the presence of DMSO (final concentration of 1.14%) did not affect the enzyme activity.

2.5.3. Antioxidant properties

2.5.3.1. SOD assay. The SOD mimetic activity was determined by a non-enzymatic method [9]. In this method, the system (PMS, phenazine methosulfate)/(NADH) produces the superoxide anion radical. The system contains 0.5 mL of sample, 0.5 mL of 1.404 mM NADH, and 0.5 mL of 300 μM NBT (nitroblue tetrazolium) in 0.05 M phosphate buffer (pH 7.5). After incubation at 25 °C for 15 min, the reaction starts by addition of 0.5 mL of 120 μM PMS. The solutions of complex were prepared in DMSO before adding the phosphate buffer to obtain the desired final concentrations. The final DMSO to buffer concentration ratio never exceeded 5:100. Then, the reaction mixture was incubated for 5 min at 25 °C. For comparative purposes, PTU was tested under the same experimental conditions. The results were determined by reading the absorbance at 560 nm. The amount of compound that produced a 50% inhibition of NBT reduction was obtained from a plot of percentage of inhibition versus compound concentration.

2.5.3.2. Scavenging of the hydroxyl radical. The ascorbate-iron-H_2O_2 system was used for hydroxyl radical's generation. The reaction mixture contains 3.75 mM 2-deoxyribose, 2.0 mM H_2O_2, 100 μM $FeCl_3$, and 100 μM EDTA without or with the tested compounds in 20 mM KH_2PO_4-KOH buffer, pH 7.4. The reaction was triggered by addition of 100 μM ascorbate and the mixture was incubated at 37 °C for 30 min. Solutions of $FeCl_3$, ascorbate, and H_2O_2 were made up in deaerated water immediately before use. Thiobarbituric acid method was applied to evaluate the extent of deoxyribose degradation by hydroxyl radical [2].

2.6. *Antibacterial and antifungal assays*

2.6.1. Antibacterial activity. Antimicrobial activity was evaluated by the minimum inhibitory concentration (MIC) on five strains of bacteria derived from the American Type Culture Collections (ATCC), namely *Escherichia coli* (ATCC 35218), *Pseudomonas aeruginosa* (ATCC 27853), *Staphylococcus aureus* (ATCC 25923) and *Enterococcus faecalis* (ATCC 29212). The MIC values were determined using the agar-dilution method. The cultivation/assay medium for all strains was Mueller Hinton Broth or Agar (MHB, MHA). The inoculum of bacterial strains was prepared from 18 h-old broth cultures. A McFarland 0.5 suspension was prepared for each microorganism and a 1:10 dilution was made prior to inoculation (~10^7 colony forming units (CFU) per milliliter). For

the agar-dilution method, PTU and $[Cu(PTU)_2]_2$ were dissolved in 50% aqueous-DMSO. All these solutions were sterilized by filtration using membrane filters with pore size 0.22 μm. Serial two-fold dilutions were prepared from the stock solution in molten MHA medium and cooled to 45 °C to obtain the desired final concentrations. Dosage of each chemical started from 2.93 μg/mL and continued until 1500 μg/mL (stopping criterion). Then, the inoculum of 2 μL of the germ suspensions was streaked onto the plates and incubated aerobically at 37 °C for 24 h. Inhibition of bacterial growth in the plates (45 × 15 mm) containing tested solutions was judged by comparison with growth in blank control plates. The MIC value was defined as the lowest dilution of the complex that inhibited visible growth of the test organism. A single colony or a faint haze caused by the inoculum should not be read as growth. Each analysis was carried out three times. An agar plate without antifungal agent and containing the same volume of DMSO was established as sterility and organism growth controls. In our experimental conditions the bacterial strains were not affected by DMSO.

2.6.2. Antifungal activity. Antifungal activity was evaluated by the MIC on three strains of fungus (*Candida parapsilosis* ATCC 22019, *Candida tropicalis* and *Candida albicans* of clinical isolates). The MIC values were determined using the agar dilution method. The cultivation/assay medium for all strains was Mueller Hinton broth or Agar (MHB, MHA) [20]. For the agar dilution method, aqueous solutions of the ligand were prepared. $[Cu(PTU)_2]_2$ was dissolved in DMSO. All these solutions were sterilized by filtration. Serial two-fold dilutions were prepared from the stock solution in molten MHA medium and cooled to 45 °C to obtain the desired final concentrations. Dosage of each chemical started from 1.46 μg/mL and continued until 1500 μg/mL (stopping criterion). Then, the inoculum of fungal strains was adjusted to 0.5 Mc Farland (~10^8 CFU per milliliter) and 2 μL of this suspension was streaked onto the plates and incubated aerobically at 37 °C for 48 h [21]. Inhibition of microbial growth in the plates containing the tested solutions was judged by comparison with growth in blank control plates. A negative control (sterility) consisting of uninoculated broth containing the same volume of DMSO was also included as organism growth controls. Bacterial strains were not affected by DMSO for each assay in our experimental conditions.

2.7. ***Carrier experience: interaction of the metal complex with albumin serum bovine (BSA)***

2.7.1. Binding affinity by fluorescence spectroscopy. BSA was dissolved in Tris–HCl (0.1 M, pH 7.4) buffer to attain a final concentration of 4% w/v (~0.6 mM). PTU and Cu-PTU solutions were added dropwise to the 2% w/v BSA solution (~0.3 mM) to ensure formation of a homogeneous solution and to obtain the desired concentrations of 0.05-0.50 mM. Adequate solubility was reached under these experimental conditions in which the compounds did not show any fluorescence intensity that could interfere with the measurements. For each sample and concentration, three independent replicates were performed. These solutions were used for the fluorescence measurements that were carried out on a Perkin–Elmer LS-50B luminescence spectrometer (Beaconsfield, England) equipped with a pulsed Xenon lamp (half peak height <10 µs, 60 Hz), an R928 photomultiplier tube and a computer working with FL Winlab software. Both excitation and emission slits were set at 5 nm throughout this study. BSA 2% w/v was titrated by successive additions of PTU and Cu-PTU solutions from 0.05 to 0.50 mM and the fluorescence intensity was measured (excitation at 280 nm and emission at 348 nm) at 25 °C.

The fluorescence quenching data were analyzed by the well-known Stern-Volmer equation (Eq. (1)) [9, 22] and the modified Stern-Volmer Eq. (2) to confirm the quenching mechanism,

$$F_0/F = 1 + K_{sv}[Q] \quad (1)$$

$$F_0/F_0\text{-}F = 1/f_a + 1/f_a K_{sv}[Q] \quad (2)$$

where F_0 and F denote the steady-state fluorescence intensities in the absence and presence of the quencher, respectively. K_{SV} is the Stern–Volmer quenching constant, f_a is the fraction of the initial fluorescence which is accessible to the quencher, [Q] is the concentration of the quencher and f_a is the fraction of accessible fluorescence [22]. K_{sv} has been determined by applying linear regression to the plot of F_0/F vs [Q] or F_0/F_0-F vs [Q]. In a certain concentration range, the curve of F_0/F versus [Q] (Stern-Volmer curve) should be linear if the quenching type is single static or dynamic. If the quenching type is a combined one (both static and dynamic), the Stern-Volmer plot presents an upward curvature.

The apparent static binding constant (K_a) and the binding site value (n) were calculated from the well-known equation by plot of log (F_0–F)/F vs log [Q]:

$$\log (F_0\text{-}F)/F = \log K_a + n \log [Q] \quad (3)$$

The value of "n" is helpful to know the number of binding sites and to locate the binding site in BSA for the drug.

2.7.2. Conformation changes on protein structure by UV-vis and vibrational spectroscopies. FT-IR spectra of the freeze-dried powdered samples were measured with a Bruker IFS 66 FT-IR spectrophotometer from 4000 to 400 cm^{-1} as KBr pellets. For data processing, spectra of the buffer were collected under the same conditions. Then, the spectrum of the buffer was subtracted from those of the samples to get the FT-IR spectra of the modified proteins. Thermoscientific DXR Smart Raman instrument equipped with a CCD detector at a resolution between 2.7-4.2 cm^{-1} with a grating groove density of 900 lines/mm was used. Spectra were recorded at room temperature with a laser power of 500 mW and a spectral resolution of 6 cm^{-1}. Each spectrum was obtained after collecting and averaging 1000 scans in order to obtain spectra with high signal-to-noise ratio. FT-Raman spectra were plotted as intensity (arbitrary units) against Raman shift in wavenumber units (cm^{-1}). All spectra were vector normalized in the whole range (4000–500 cm^{-1}). In order to improve signal-to-noise ratio in FTIR and Raman spectra, Tris–HCl buffer, BSA solutions and PTU and Cu-PTU solutions were lyophilized. Solutions were prepared in the same experimental conditions as fluorescence spectroscopy studies. As with other proteins, particularly globulins, FT-Raman spectra of protein solutions and freeze-dried powders are almost identical, therefore, freeze drying does not affect protein conformation. This behavior was taken into account during the experimental procedure. The plotting, processing, normalizations, manipulations, and evaluation of spectra (FT-IR and Raman) were carried out using the OPUS software (Bruker Optics, Germany). Band intensities were calculated after a linear baseline correction performed with an integration method developed within OPUS software. The intensity values obtained for the tyrosine doublet were calculated taking into account the local baseline of each peak (830 and 850 cm^{-1}). Bands of the major vibrational motions of the side chains or the peptide backbone were assigned by comparison to Raman data reported in the literature [23]. Determination of secondary structure of BSA and the samples containing PTU and Cu-PTU solutions with BSA was carried out on the basis of the procedure described by Byler and Susi [24]. In a usual procedure the Amide I region (1700-1600 cm^{-1}) was used to investigate the secondary structure of BSA in a quantitative manner. The frequencies, the number of peaks to be fitted, and the half-width of each peak to start least-square

iterative curve-fitting procedures were those obtained from the second derivative of the original spectra. The areas of the bands were calculated by integration of the corresponding fitted band. A straight baseline passing through the ordinates at 1700 cm^{-1} and 1600 cm^{-1} was adjusted as an additional parameter to obtain the best fit. The curve-fitting procedure was performed by stepwise iterative adjustment towards a minimum root mean-square error of the different parameters determining the shape and position of the absorption peaks. It was carried out by assuming an initial mixed Lorentzian–Gaussian line-shape function, with full width band at half-height (FWHH) of 13-18 cm^{-1} and a maximum resolution factor. Baseline corrections, normalization, derivation, curve fitting and area calculation were carried out by means of Grams/32 (Galactic Industries Corporation, USA) software, OPUS 3.1 and Perkin-Elmer software. The resulting fitted curve was analyzed taking into account the band assignment for the secondary structure previously reported: α-helix, 1658-1650 cm^{-1}; β-sheets, 1637-1613 cm^{-1}; turns, 1673-1666 cm^{-1}; random coil, 1645-1637 cm^{-1}; and β-antiparallel, 1695-1675 cm^{-1} [10]. In order to calculate the percentage contribution of the different types of conformations to the area of all the components, bands assigned to a given conformation were summed and divided by the total Amide I area. All analyses were performed in three independent experiments, and the results were reported as averages of these replicates. A Bruker ESP300 spectrometer operating at X and Q-bands, and equipped with standard Oxford low temperature devices was used to record EPR spectra of the compounds at different temperatures. The magnetic field was measured with a Bruker BNM 200 gaussmeter, and the frequency inside the cavity was determined by using a Hewlett-Packard 5352B microwave frequency counter. Anisotropic X-band EPR spectra of frozen solutions were recorded at 140 K, after addition of 10% ethylene glycol to ensure good glass formation. A computer simulation of the EPR spectra was performed using SimFonia software [8]. The concentration ratios were the same as those used in the fluorescence measurements.

The solutions (0.50 mM of the compounds: 2% w/v BSA) were also assayed by UV–vis electronic spectroscopy. Electronic absorption spectra were recorded with a Hewlett-Packard 8453 diode-array spectrophotometer using 1 cm quartz cells in the 200–800 nm range. Buffer solutions were used as reference. Three independent replicates of BSA solution and the corresponding compounds were measured.

3. Results and discussion

3.1. *Structural characterization*

3.1.1. FTIR spectroscopy. Propylthiouracil (figure 1) presents three potential coordination sites: carbonyl (C=O), -N-H (amine) and C=S (thione) groups. Usually, such ligands as methimazole are in the thione tautomer form in solid state but in solution thione-thiol isomerism could be present depending on factors like pH, metal nature, solvent effects, *etc*. The infrared spectra of PTU (table 2) confirm that in the solid the thione sulfur conformation is predominant. The thione form is confirmed by the absence of ν(SH) at *ca*. 2500 cm^{-1} and the presence of the ν(NH) band at 3089 cm^{-1} (table 2) [10]. The band related to ν(C=O) at 1702 cm^{-1} is also present. In IR spectra of the complex, the position of the latter band remains unaltered discarding interaction of the metal *via* this group [25].

Changes arising from involvement of the –N(19)H–C(11)(=S(18))–N(6)H– group [26] in the coordination to the metal center can be observed (table 2). As expected, and taking into account the less polar character of the thiocarbonyl (C=S), ν(C=S) occurs at lower wavenumbers than ν(C=O). When the carbon is directly linked to nitrogen, ν(C=S) is strongly coupled generating a number of different bands in the region 1570–700 cm^{-1} that contain some contribution from ν(C=S). In compounds of this type, the thioamide group normally gives four bands at 1570–1395, 1420–1260, 1140–940 and 800–700 cm^{-1} and these bands are known as the 'thioamide I, II, III and IV' bands, respectively. Bands I and II have little C=S content and originate mainly in C=N and NH deformation modes while bands III and IV have significant C=S content [10]. These bands are used to predict the mode of coordination of the heterocyclic thione complexes.

The monodentate sulfur donating character of PTU is evident by comparison with the position of the four thioamide bands in the IR spectra for the complex and the free ligand. In particular, the shift to higher frequencies of the thioamide I band which has a higher ν(CN) character, has been assigned to metal-N coordination [27]. The balance of the π-character of the C-S and C-N bonds is perturbed upon coordination concentrating the anionic charge of the thionate sulfur and the π-electron density in the C-N thioamide bond enhancing the bridging potential of the ligand [28]. This redistribution of electronic charge densities indicates probable interaction through the adjacent N(6) to C(11)=S(18) thione. The interaction of the metal to N(19) could be discarded because the frequency of the C=O group next to it remained unaltered.

This change is also in correlation with a marked decrease in the NH band intensity, suggesting at least that one of the two NH groups in the ligand molecule are involved in coordination to the metal. According to the observed modifications of the spectral pattern of free PTU, it is possible to suggest that the NCS may be bonded to a metal through N and S or may form a bridge between the two metals coordinating by both N and S. The presence of the free thiol tautomer has been discarded due to the absence of the typical ν(SH) stretch at *ca*. 2500 cm^{-1} and the band located at 419 cm^{-1} could be tentatively assigned to the ν(Cu-N) stretch [29].

3.1.2. Electron spin resonance spectra (EPR). To obtain deeper insight into the environment around copper(II) in the complex, EPR spectroscopic studies were undertaken. Electron Spin Resonance is often employed to characterize binuclear systems. Particularly, in the case of copper(II)–copper(II) complexes EPR spectrum allows the recognition of magnetic couplings between the two ions with S=1 state. In fact, the X and Q-band EPR powder spectra of the $[Cu(PTU)_2]_2$ complex were measured at 290 K. The polycrystalline sample of $[Cu(PTU)_2]_2$ (violet) showed better resolution in the Q-band (figure 2) denoting clearly the presence of an isolated Cu(II)-dimer having a strong zero-field splitting.

The best fit was obtained for spin Hamiltonian parameters of $g_{\|} = 2.285$, $g_{\perp} = 2.053$, $A_{\|} = 170\times10^{-4}$ cm^{-1}, $A_{\perp} = 65\times10^{-4}$ cm^{-1}, $D = 0.2650$ cm^{-1}. The low value for $g_{\|}$ is in concordance with an elongated octahedral environment. Taking into account the empirical factor *f* ($f = g_{\|}/A_{\|}$) that represents the index of tetrahedral distortion, the calculated *f* value of 134 falls in the range of the complexes with square planar geometries [30]. The value of the parallel component of the hyperfine coupling constant is consistent to that found in copper complexes with chromophores containing N and S donors in the coordination sphere [14, 16]. The g values obtained from the spectral fitting can be tested by determination of the G parameter [31] to decide if they are actually molecular parameters:

$$G = \frac{g_{\|} - g_0}{g_{\perp} - g_0}$$

This parameter is greater than 4 when the exchange g values are equal to the molecular ones. In this case, the calculated G value is 5.6, indicating that only the interactions between magnetically equivalent or ferrodistortively ordered chromophores are operative.

The EPR signal is very clear about interaction between the two copper centers forming the dimer. This interaction is much greater than the possible interdimer coupling which significantly affects the EPR signal, broadening the lines [32]. This type of EPR signal appears when there is a short distance between the Cu…Cu centers (2.6-3.5 Å) or a very good overlap of the Cu…Cu orbitals takes place. This is more often probable in a planar coordination than in a tetrahedral one. Due to presence of weak axial interactions, dinuclear or polynuclear chains with the formation of equatorial bridges are usually expected in square based Cu(II) complexes [33].

In brief, considering the chemical analysis, the presence of the dimeric complex identified by EPR spectroscopy, the interaction *via* S and N atoms observed by FTIR and EPR measurements together with the reflectance spectrum (see above), it is possible to assume that the copper(II) ion exhibits a planar geometry, where two ligands are bidentate bridging (N and S atoms) and the other two ligands also coordinated through N and S. The asymmetric character of the S,N-chelating heterocyclic thionates generates a large number of geometric isomers [34]. Bidentate coordination has previously been performed in several complexes with this type of ligand. The bidentate coordination mode in metal complexes has been widely reported including bridging coordination mode between two metal centers [33, 35].

3.1.3. Solid diffuse reflectance spectrum and solution UV-vis and EPR spectral studies. The diffuse reflectance spectrum of $[Cu(PTU)_2]_2$ (figure 3, solid line) showed bands at 736 nm and 531 nm. The broad band at low energy was assigned to the d-d transitions of the copper(II) in square coplanar environment (450-830 nm region, rather asymmetric due to d^9 configuration Jahn-Teller effect) [36, 37]. Noticeable, the other band around 500 nm has high intensity. Various planar, tetragonal and five-coordinate Cu(II) complexes have equatorial $S^* \rightarrow Cu(II)$ bonding with a prominent LMCT band [38]. This band (figure 3, dotted line) is also present in ethanol solution, in which the complex is sparingly soluble and the molar absorption coefficient value cannot be calculated (the spectrum is shown only for comparative purposes). On the contrary, the complex is soluble in DMSO, and the UV-visible spectrum (figure 3, inset) showed bands at 808 nm (ε = 122 $M^{-1}cm^{-1}$) and 494 nm (ε = 197 $M^{-1}cm^{-1}$). The d-d band shifting toward higher wavelengths can be attributed to the breakdown of the dimer complex resulting in access of solvent in the coordination sphere of Cu(II). The presence of a band at ~500 nm indicates the presence of $S^* \rightarrow Cu(II)$ bonding. The lowering in the intensity of this band has been suggested as a consequence

of the change from equatorial to apical position of the thioether-Cu(II) bonding [27]. Then, a possible change of the coordination mode from square coplanar in the solid state to octahedral in DMSO solution can be suggested. The data obtained from the solution EPR spectrum confirms this hypothesis showing Hamiltonian parameters of $g_{\|} = 2.315$, $g_{\perp} = 2.060$, $A_{\|} = 152\times10^{-4}$ cm^{-1}, $A_{\perp} = 14\times10^{-4}$ cm^{-1}, $A(2N) = 14\times10^{-4}$ cm^{-1}. The value of the *f* factor of 152.2 is an indication that the copper(II) retains two ligands in the coordination sphere.

In view of the *in vitro* biological studies, the stability of the complex was evaluated in DMSO. Under these conditions, the chemical species formed on dissolution was stable during 1 h (not shown).

Note: The mathematical determination of the concentration for the dimeric complex match with the mathematical calculations of the concentration of the complex per mole of copper atoms. Considering that the dimeric complex dissociates in DMSO solution into the monomeric complex Cu(PTU)$_2$, for UV-vis and EPR solution spectra and for "in vitro" experiments, solution concentrations have now been expressed per copper ion.

3.1.4. Dissolution profile assay. The dissolution performances of the propylthiouracil (PTU) and $[Cu(PTU)_2]_2$ were determined in different dissolution media. The proportion used in preparation of capsules in both PTU and the complex simulates the amount of propylthiouracil in formulations that are sold in Chile, Brazil, Bolivia, United States, among others, since the pharmaceutical treatments with this drug are not allowed in our country. Figure 4 shows the dissolution profiles using 100 rpm. The results indicate that the PTU has excellent dissolution: H_2O (99.4%), simulated gastric medium (97.8%), HCl (97.5%) and sodium lauryl sulfate (93.3%), but only 40% of dissolution with phosphate buffer. In general, the percentage of the dissolution increases with the time in all cases until a constant value gets an asymptote where the value is maintained constant for several minutes reaching to thermodynamic equilibrium. $[Cu(PTU)_2]_2$ shows poor solubility in H_2O (3.5%), phosphate buffer (4.5%), HCl (6.6%), and simulated gastric environment (10.8%). The highest percentage of the dissolution of the complex was achieved using sodium lauryl sulfate as solvent (28.4%), but no thermodynamic equilibrium was reached until 60 minutes.

In view of the obtained results in the future other pre-formulation studies to enhance the solubility and dissolution rate of the complex using solid dispersions (DS), for the development of pharmaceutical forms.

3.1.5. Biological activities

3.1.5.1. Phosphatases inhibition experiments. Interest of researchers in inhibition of enzymes has been growing because they found abnormally high levels in serum of certain enzymes in several diseases (*e.g*. accumulation of target proteins) [39]. In particular, an excess of the reference range of alkaline phosphatase can be associated with certain medical conditions as bone and Paget's diseases, cancer (bone metastases, breast carcinoma, colon, Hodgkin lymphoma), hyperthyroidism, celiac disease, sarcoidosis, *etc*. [40]. Another point of interest is that alkaline phosphatase is usually produced by microorganisms (*e.g*. bacteria) only during phosphate starvation due to the requirement of the inorganic phosphate anion (Pi) which is essential for their survival [41]. In consequence by controlling ALP levels, the microorganism action could be restricted. In this context, the development of enzyme inhibitors is of great interest to act on the overproduction of the enzyme.

The activity of ALP in the presence of copper(II) cation has been well documented [42-46]. Most showed that copper(II) did not display significant inhibitory effect while in others ALP activity was reduced. We have shown that copper(II) produced a weak inhibitory action on ALP activity [10]. For that reason, the inhibitory activity of $[Cu(PTU)_2]_2$ and the free ligand are shown at this time (figure 5(A)). The results show that the free ligand had no effect on the ALP enzyme activity. However the inhibition exerted by $[Cu(PTU)_2]_2$ takes place at higher concentrations reaching a 45% inhibition at 500 µM concentration. Then it could be suggested that copper(II) complexation produces a metal-drug synergic behavior improving the inhibitory ability on ALP having specific action as phosphatase inhibitor. This behavior is opposite to the observed in AcP experiments (figure 5(B)) in which both compounds acted in a similar way inhibiting 32-34% of the enzyme activity.

3.1.5.2. Antioxidant activity. The correlation between Graves' disease and the formation of reactive oxygen species (ROS) and other free radicals has been reported [8]. It was also revealed that hyperthyroidism-induced dysfunction of the respiratory chain in mitochondria leads to ROS production and generates an increase of the SOD activity in erythrocytes. At high concentrations, ROS can be intermediaries to injure cell structures, lipids, membranes, proteins and nucleic acids (oxidative stress). In addition, it was proved that serum levels of lipid peroxides in hyperthyroid patients were decreased after treatment with PTU [47]. These findings suggest that PTU may act as

a scavenger of oxygen free radicals or may directly protect lipids from peroxidative attack. Based on these results, the antioxidant activities of PTU and its copper complex against superoxide and hydroxyl radicals were determined.

The dismutation power of PTU and $[Cu(PTU)_2]_2$ on superoxide was determined using a non-enzymatic assay at pH 7.5. The scavenger activity is shown in figure 6(A). Neither PTU nor the complex has ability to dismutate the $O_2^{\bullet-}$ radical. The present results for PTU indicate superoxide radical anion scavenging activity exhibited when superoxide radicals were produced from action of xanthine oxidase on xanthine [47]. Under the experimental condition of that work, PTU (at a concentration range of 10-200 µM) caused only a small decrease in the rate of superoxide induced cytochrome c reduction.

The reactivity of PTU with hydroxyl radicals was also proved (figure 6(B)). In this case, a significant increase in the disruption of $OH^{\bullet}$ radical was observed for PTU and its copper(II) complex. The activity is higher for the complex reducing 71% in the presence of the radicals at a concentration of 10 µM while PTU reduced only 52% at the same concentration. This behavior correlates with that observed by Hicks *et al*. in which PTU behaved as an efficient hydroxyl radical scavenger [47]. The data obtained here reinforces the idea of antioxidant activity exhibited by PTU on $OH^{\bullet}$ radicals and demonstrated that this action is efficiently improved with complexation with copper(II) at 10 µM concentration.

3.1.5.3. Antibacterial and antifungal assays. Earlier studies have shown that some drugs exhibit increased biological activity when administered as metal chelates rather than as organic compounds. The improvement of their antimicrobial effect in metal complexes is explained based on "Tweedy chelation theory" and the "Overtone concept" [48].

Several copper complexes have been effective as antibacterial agents regardless of the geometric arrangement. For instance, octahedral monomer ($Cu(II)N_6$) [49], five-coordinate dimers ($Cu(II)O_4N$ [50], $Cu(II)N_2O_3$ [51]) and square planar geometry ($Cu(II)N_2O_2$ [52]) among others.

In our investigations, the antimicrobial profile of ($CuCl_2{\cdot}2H_2O$), PTU and the complex Cu-PTU have been studied against gram-positive and negative bacteria and fungi by the agar dilution method. The results of the antimicrobial activities are summarized in table 3. Pointing that the antimicrobial activity could be significant (MIC ≤ 100 µg/mL), moderate (MIC between 100–500 µg/mL), weak (MIC between 500-1000 µg/mL) and that values of MIC over 1000 µg/mL

indicate no antibacterial activities [10], the Cu-PTU complex has higher potency against *E. faecalis* and *S. aureus* and for all the three studied fungi in comparison with PTU and the copper salt.

The complex is more active against Gram-positive bacteria while Gram-negative bacteria are more resistant. This behavior could be related to the presence of a double membrane in the bacterial cell. Even though all bacteria have an inner cell membrane, Gram-negative bacteria have a unique outer membrane which rejects drugs and antibiotics, more resistant to antibiotics than Gram-positive ones. In our investigation, we began to study for the first time antimicrobial activity of typical antithyroid drugs and its copper complexes. Cu-PTU behaves as antibacterial agent much better than Cu-Met ($[Cu(Met)_2(H_2O)_2](NO_3)_2 \cdot H_2O$) and Cu-Met-phen ($[Cu(Met)_2(phen)(H_2O)_2]Cl_2$) [8]. In general, there are some complexes with similar or related coordination modes that were tested as antibacterial agents but a direct comparison of the activity cannot be performed because the experimental methodologies were not the same. For instance, there are complexes with square planar geometries having analogous $Cu(II)N_2S_2$ environments [53-55], bimetallic complexes [56], compounds with a $Cu(II)NSCl_2$ donor set [57], and complexes with pyramidal and octahedral symmetries ($(Cu(II)N_2S_2(Cl))$ [58] and ($Cu(II)N_2S_2X_2$, X = halogen) [59]) that show in general improvement of the antibacterial activity of the ligand. Unfortunately, the antibacterial activity data are given as percentage or as the diameter of inhibition zone and do not allow a detailed comparison. In this search, an octahedral thione Cu(II) complex [60] ($CuL_2 \cdot 4H_2O$, L = 1-amino-5-benzoyl-4-phenyl-1*H*-pyrimidine-2-thione) and other four-coordinate copper(II)-*bis*(thiosemicarbazonato) complexes [61] were examples of complexes having the same set of atoms in the equatorial coordination sphere (table 3). Cu-PTU is almost three times more active on *S. aureus* and *C. parapsilosis* than the thione Cu(II) complex, but Cu(II)-thiosemicarbazone complexes were more efficient than Cu-PTU on *S. aureus* and especially on *E.coli* strain.

It could be suggested that Cu-PTU was not efficient to enter the bacterial cytoplasm on *E. coli* in comparison with Cu(II) thiosemicarbazone complexes, but it could enter more rapidly than $CuCl_2$ salt on the other strains having significant antimicrobial action. Synergetic behavior was produced by copper(II) coordination to PTU ligand increasing its lipophilicity in these bacterial and fungal strains.

3.1.5.4. Bovine serum albumin interactions. Our earlier studies established the binding affinity of bovine serum albumin with anti-thyroid methimazole molecule [9]. This information led us to

investigate the extent and nature of interactions of PTU and its copper(II) complex with serum albumin, the binding constant and binding sites and the drug-induced conformational changes in protein, using fluorescence, Raman and FTIR spectroscopies. In fact, the objective is a better understanding of important binding parameters since the general distribution, metabolism and efficacy of many drugs in the body are correlated with their affinities towards serum albumin. Previous fluorescence studies have established the binding affinity of PTU to human serum albumin (72.46 μM) being moderate but enough to be carried by HSA in blood [62].

3.1.5.4.1. Fluorescence experiments. Macromolecule fluorescence experiments provide information of the binding of small molecules to proteins, such as binding mechanism, binding mode, binding constants and binding sites. Fluorescence intensity of a compound can be decreased by a variety of molecular interactions and that this decrease in intensity is known as "quenching". Many Cu(II) complexes produced quenching on the characteristic band derived from the intrinsic fluorescence of BSA with this effect attributed to static interaction and compound formation between BSA and the metal complex [63, 64].

In our experiments, this effect was evaluated by measurement of intrinsic fluorescence intensity of BSA before and after addition of PTU and Cu-PTU from 300–500 nm upon excitation at 296 nm. The effect of the compounds on BSA fluorescence intensity is shown in figure 7 ((A) PTU, (B) Cu-PTU). When different amounts of PTU and Cu-PTU solutions were titrated with a fixed concentration of albumin a remarkable decrease in the fluorescence intensity of BSA is produced, indicating strong interaction of both compounds. In titration with PTU and BSA (figure 7(A)) a small λ_{em} shift to higher wavelengths (a red shift from 348 to 354 nm) with increasing ligand concentration is observed. This behavior implies that binding of PTU to BSA occurs and the microenvironment around the chromophore of the protein is changed. The observed spectral λ_{em} shift is an indication that the conformation of the protein can be affected by the addition of drugs and can be attributed to the exposure of tryptophan residue (Trp^{214} site) to a more polar environment [33, 65]. For Cu-PTU-BSA system the observed effect is higher than for PTU-BSA at the same concentration values; λ_{em} shifted from 348 nm (basal) to 363 nm (0.125 mM) and near to 400 nm at the maximum concentration value. This change indicates a stronger quenching effect of the complex together with modification in the structure of the protein.

The extent of the changes was first analyzed using the well-known Stern–Volmer Eq. (1) (see Experimental section). For PTU-BSA the plot showed a linear dependence suggesting that only

one process (dynamic or static one) took place while for Cu-PTU-BSA the plot showed positive deviation (concave towards the "y" axis) indicating the presence of both static and dynamic quenching. Considering for the Cu-PTU system, only the data at lower concentrations in which the curve appears to be linear, the fluorescence data at room temperature were further examined using the modified Stern-Volmer equation (Eq. (2)). From the plot of F_0/F_0-F versus 1/[Q], the fraction f_a and the Stern-Volmer constant K_{sv} were obtained from the values of intercept and slope, respectively. The calculated fraction f_a values were 1.09 for PTU and 1.01 for Cu-PTU, indicating that 91.74% and 99.00% of the total fluorescence of BSA is accessible to PTU and Cu-PTU quenchers, respectively. The Stern-Volmer quenching constants at 298 K were 1.23×10^4 M^{-1} for PTU-BSA and 13.7×10^4 M^{1} for Cu-PTU-BSA. Considering the relationship between the quenching rate constant of the biomolecule K_q and the dynamic quenching constant K_{sv} ($k_q = K_{sv}/\tau_0$, where τ_0 is the average lifetime of the biomolecule without quencher), and taking into account that the fluorescence lifetime of the biopolymer is 10^{-8} s [38], k_q can be calculated as 1.23×10^{12} M^{-1} s^{-1} and 13.7×10^{12} $M^{-1}s^{-1}$, respectively. The maximum scatter collision quenching constant (k_q) of various quenchers with the biopolymer is assumed to be 2×10^{10} $M^{-1}s^{-1}$ [38]. In this experiment both rate constants of the protein quenching procedure initiated by PTU and Cu-PTU are greater than k_q for the scatter mechanism suggesting the interaction of BSA with both PTU and the Cu-PTU by formation of a complex system.

Binding parameters were also evaluated by Eq. (3). In consequence, a plot of log $(F_0\text{-}F)/F$ versus log [Q] (figure 7, (C) PTU, (D) Cu-PTU) yielded the K_a and n values to be 1.51×10^6 M^{-1} (n=1.51) and 1.80×10^8 M^{-1} (n=1.85), respectively. The values of n were in both cases greater that 1 and for the Cu-PTU complex suggest the existence of two binding sites in BSA.

3.1.5.4.2. Monitoring and evaluation of the conformational induced changes on BSA and the complex-BSA environment by spectroscopic techniques. For confirmation of the structural changes of BSA by addition of PTU and the Cu-PTU complex, we measured the UV-vis absorbance spectra at the same experimental conditions as for the fluorescence experiments. The spectrum of the BSA solution showed the typical band at ~280 nm generated by the aromatic amino acid side-chains (phenylalanine, histidine, tryptophan (Trp) and tyrosine (Tyr)) (figure 8) [35]. This typical band is used to study the tryptophan and tyrosine residue alterations. From figure 8 the baselines of the UV-vis absorbance spectra at 250-320 nm are raised and there is no significant change in the position of the maximum of the band when concentration is increased from 0.025 to 0.500 mM.

This increase of intensity, which is greater for the metal complex, is associated with the interaction between the compounds and BSA changing the protein conformation due to the aromatic residues.

From the FT-Raman spectra, additional changes were observed. At first, the typical tyrosine doublet was analyzed. In comparison with free BSA, PTU did not alter the $I_{850/830}$ ratio giving a value of 0.34±0.01 close to the control. Modifications of this doublet are observed after interaction with Cu-PTU giving the ratio ($I_{850/830}$ = 0.26±0.01) approximately 20% lower than the BSA control and the ligand. This behavior suggests an increase in buriedness and possible involvement of tyrosyl residues in inter- or intramolecular interactions. In contrast to the observations for BSA and the ligand, the characteristic tryptophan band (880 cm^{-1}) clearly appeared in the complex interaction, suggesting that this residue became exposed from a buried hydrophobic microenvironment [9, 66]. Taking into account the band assignment for the secondary structure in FTIR spectra, each polypeptide conformation could be related to a higher or lower degree of protein folding. Both α-helix conformations (solvated and unsolvated) are more compact structures and the random coil conformation is less compact and more disordered [67].

Finally the environment of the metal complex interacting with the albumin was studied by EPR spectroscopy. The simulation of the spectrum (spin Hamiltonian parameters: $g_{\|}$ = 2.26, $g_{\perp}$ = 2.061, $A_{\|}$ = 185×10^{-4} cm^{-1}, $A_{\perp}$ = 2×10^{-4} cm^{-1}, (A_{iso} = 63×10^{-4} cm^{-1}, g_{iso} = 2.127) proposes interaction of the complex with the protein residues being the hyperfine coupling constant value ($A_{\|}$) coincident with additional nitrogens in the coordination sphere of the metal center (probably belonging to the exposed Trp residues) [68]. Partial dissociation of the metal complex was discarded because of the presence of a single solution species with Hamiltonian parameters very different to the well-known Cu(II) in the N terminus-site VI of the BSA.

4. Conclusion

We proved new pharmacological activities for propylthiouracil, and the first time that a copper(II) complex with propylthiouracil was prepared as a binuclear metal complex. The new $[Cu(PTU)_2]_2$ complex has been characterized by several spectroscopies (FTIR, EPR, UV-visible and diffuse reflectance) and by elemental analysis, dissolution profiles and stability studies. We demonstrated the potential of the monomeric complex obtained after $[Cu(PTU)_2]_2$ dissolution and the PTU to act as a good anti-$OH^{\bullet}$ radical showing significant disruption of this species. While PTU did not show antimicrobial activity, the monomeric complex behaved as a very active antibacterial against

E. faecalis and *S. aureus* and as a strong antifungal agent on *C. albicans*, *C. tropicalis* and *C. parapsilosis*. In addition, its demonstrated ability to inhibit phosphatase alkaline (45% of inhibition at 500 μM concentration) could be associated with its antibacterial effect, a good synergetic action to attack microorganisms by killing them including phosphate starvation strategy. Considering the potential use of this complex as a pharmaceutical agent, we have also studied the albumin binding affinity. The experiments showed that this complex has a constant binding value two hundred times higher than the ligand occupying two binding sites. Conformational analysis by FTIR and Raman spectroscopies suggested that the interaction of the complex was *via* tryptophan residues, coincident with the EPR results that proposed additional nitrogens in the coordination sphere of the metal center. Based on this study, it is hypothesized that $[Cu(PTU)_2]_2$, in which the bioactive species is the monomeric complex, would be a promising candidate for further pharmaceutical evaluation acting as an antioxidant, antimicrobial and phosphatase alkaline inhibitor agent.

Acknowledgements

This work was supported by UNLP (Universidad Nacional de La Plata, X739, X736), UNCAUS (Universidad Nacional del Chaco Austral, PI N°25), CONICET (Consejo Nacional de Investigaciones Científicas y Técnicas, PIP-0611), CICPBA (Comisión Nacional de Investigaciones Científicas y Técnicas de la Provincia de Buenos Aires, N^0 813/13) and ANPCyT (Agencia Nacional de Promoción Científica y Técnica, PICT-2013-0569), Argentina. EGF and LGN are research fellows of CONICET. PAMW is a research fellow of CICPBA, Argentina. JJMM is a fellowship holder from CONICET.

References

[1] S. David, M.D. Cooper. *New Engl. J. Med.*, **352**, 905 (2005).

[2] C-T. He, A-T. Hsieh, D. Pei, Y-J. Hung, L-Y. Wu, T-C. Yang, W-C. Lian, W-S. Huang, S-W. Kuo. *Clin. Endocrinol.*, **60**, 676 (2004).

[3] O. Diav-Citrin, A. Ornoy. *Teratology*, **65**, 38 (2002).

[4] D. Das, G. Roy, G. Mugesh. *J. Med. Chem,*, **51**, 7313 (2008).

[5] G. Roy, M. Nethaji, G. Mugesh. *J. Am. Chem. Soc.*, **126**, 2712 (2004).

[6] T.W. Petry, T.E. Eling. *J. Biol. Chem.*, **262**, 14112 (1987).

[7] B. Kasraee, A. Hugin, C. Tran, O. Sorg, J-H. Saurat. *SID*, **122**, 1338 (2004).

[8] N.M. Urquiza, M.S. Islas, L. Dittler, M.A. Moyano, S.G. Manca, L. Lezama, T. Rojo, J.J. Martínez Medina, M. Diez, L. López Tévez, P.A.M. Williams, E.G. Ferrer. *Inorg. Chim. Acta*, **405**, 243 (2013).

[9] N.M. Urquiza, L.G. Naso, S.G. Manca, L. Lezama, T. Rojo, P.A.M. Williams, E.G. Ferrer. *Polyhedron*, **31**, 530 (2012).

[10] N.M. Urquiza, S.G. Manca, M.A. Moyano, A. Arrieta Dellmans, L. Lezama, T. Rojo, L.G. Naso, P.A.M. Williams, E.G. Ferrer. *BioMetals,* **23**, 255 (2010) and references therein.

[11] K. Komosinska-Vasseva, K. Olczyka, E.J. Kucharz, C. Marcisz, K. Winsz-Szczotka, A. Kotulska. *Clin. Chim. Acta*, **300**, 107 (2000).

[12] V. Bacic-Vrca, F. Skreb, I. Cepelak, L. Mayer, Z. Kusic, B. Petres. *Clin. Chem. Lab. Med.*, **43**, 383 (2005).

[13] M. Abalovich, S. Llesuy, S. Gutierrez, M. Repetto. *Clin. Endocrinol.*, **59**, 321 (2003).

[14] R.H. Lindsay, H.Y. Aboul-Enein, D. Morel, S. Bowen. *J. Pharm. Sci.*, **63**, 1383 (1974).

[15] A. Taurog, M.L. Dorris, W-X. Hu, F.S. Guziec. *Biochem. Pharmacol.*, **49**, 701 (1995).

[16] K. Paizanos, D. Charalampou, N. Kourkoumelis, D. Kalpogiannaki, L. Hadjiarapoglou, A. Spanopoulou, K. Lazarou, M.J. Manos, A.J. Tasiopoulos, M. Kubicki, S.K. Hadjikakou. *Inorg. Chem.*, **51**, 12248 (2012).

[17] F. Isaia, M.C. Aragoni, M. Arca, C. Caltagirone, C. Castellano, F. Demartin, A. Garau, V. Lippolis, A. Pintus. *Dalton Trans.*, **40**, 4505 (2011).

[18] Drug Committee of the Spanish Association of Pediatrics. Pediamécum. Edition 2012. Propylthiouracil. Available in: http://www.pediamecum.es.

[19] U. Blum, G. Schwedt. *Anal. Chim. Acta*, **360**, 101 (1998).

[20] T. Suksrichavalit, S. Prachayasittikul, C. Nantasenamat, C. Isarankura-Na-Ayudhya, V. Prachayasittikul. *Eur. J. Med. Chem.*, **44**, 3259 (2009).

[21] M.C. Rodríguez-Argüelles, E.C. López-Silva, J. Sanmartín, P. Pelagatti, F. Zani. *J. Inorg. Biochem.*, **99**, 2231 (2005).

[22] J.R. Lakowicz, Principles of Fluorescence Spectroscopy, Plenum Press, New York (1999).

[23] A.T. Tu, Raman Spectroscopy in Biology, Principles and Applications, John Wiley & Sons Inc., New York (1982).

[24] D.M. Byler, H. Susi. *Biopolymers*, **25**, 469 (1986).

[25] S. Mansy, R. Stuart Tobias. *Inorg. Chem.*, **14**, 287 (1975).

[26] F. Furlan Ferreira, A.C. Trindade, S. Gutierrez, A. de Oliveira, C. Paiva-Santos. *CrystEngComm*, **13**, 5474 (2011).

[27] N.A. Bell, W. Clegg, S.J. Coles, C.P. Constable, R.W. Harrington, M.B. Hursthouse, M.E. Light, E.S. Raper, C. Sammon, M.R. Walker. *Inorg. Chim. Acta*, **357**, 2091 (2004).

[28] N.A. Bell, W. Clegg, J.R. Creighton, E.S. Raper. *Inorg. Chim. Acta*, **303**, 12 (2000).

[29] V. Philip, V. Suni, M.R. Prathapachandra Kurup, M. Nethaji. *Polyhedron*, **24**, 1133 (2005).

[30] R. Pogni, M.C. Baratto, A. Diaz, R. Basosi. *J. Inorg. Biochem.*, **79**, 333 (2000).

[31] B.J. Hathaway, D. Billing. *Coord. Chem. Rev.*, **5**, 143 (1970).

[32] S.K. Hoffmann, D.K. Towle, W.E. Hatfield, P. Chaudhuri, K. Wieghardt. *Inorg. Chem.*, **24**, 1307 (1985).

[33] R. Kannappan, S. Tanasea, I. Mutikainen, U. Turpeinen, J. Reedijk. *Inorg. Chim. Acta*, **358**, 383 (2005).

[34] E.S. Raper. *Coord. Chem. Rev.*, **165**, 475 (1997).

[35] E. Block, G. Ofori-Okai. *Inorg. Chim. Acta*, **189**, 137 (1991).

[36] M. Joseph, V. Suni, M.R. Prathapachandra Kurup, M. Nethaji, A. Kishore, S.G. Bhat. *Polyhedron*, **23**, 3069 (2004).

[37] A.B.P. Lever, Inorganic Electronic Spectroscopy, Elsevier, The Netherlands (1984).

[38] H.J. Prochaska, W.F. Schwindinger, M. Schawartz, M.J. Burk, E. Bernarducci, R.A. Lalancette, J.A. Potenza, H.J. Schugar. *J. Am. Chem. Soc.*, **103**, 3446 (1981).

[39] Z. Zhang, C. Bi, S.M. Schmitt, Y. Fan, L. Dong, J. Zuo, Q. Ping Dou. *J. Biol. Inorg. Chem.*, **17**, 1257 (2012).

[40] L-F. Hsu, C. Rajasoorya. *Eur. J. Endocrinol.*, **140**, 143 (1999).

[41] P. de Prada, J. Loveland-Curtze, J.E. Brenchley. *Appl. Environ. Microbiol.*, **62**, 3732 (1996).

[42] C. Xie, R. Lu, Y. Huang, Q. Wang, X. Xu. *Bioresour. Technol.*, **101**, 3394 (2010).

[43] M.T. Mazorra, J.A. Rubio, J. Blasco. *Comp. Biochem. Phys. B*, **131**, 241 (2002).

[44] G. Renella, A.L.R. Ortigoza, L. Landi, P. Nannipieri. *Soil Biol. Biochem.*, **35**, 1203 (2003).

[45] Q-X. Chen, W-Z. Zheng, J-Y. Lin, Y. Shi, W-Z. Xie, H-M. Zhou. *Int. J. Biochem. Cell Biol.*, **32**, 879 (1989).

[46] K.P. Flint, J.W. Hopton. *Eur. J. Appl. Microbiol.*, **4**, 195 (1977).

[47] M. Hicks, L.S. Wong, R.O. Day. *Biochem. Pharmacol.*, **43**, 439 (1992).

[48] J.J. Martínez Medina, C.A. Torres, W.S. Alegre, C.A. Franca, L.L. López Tévez, E.G. Ferrer, N.B. Okulik, P.A.M. Williams. *J. Mol. Struct.*, **1100**, 366 (2015).

[49] S.M. Tailor, U.H. Patel. *J. Coord. Chem.*, **68**, 2192 (2015).

[50] R.C. Santra, K. Sengupta, R. Deya, T. Shireen, P. Dasa, P.S. Guina, K. Mukhopadhyay, S. Das. *J. Coord. Chem.*, **67**, 265 (2014).

[51] S. Caglar, E. Adiguzel, B. Sariboga, E. Temel, O. Buyukgungor. *J. Coord. Chem.*, **67**, 670 (2014).

[52] S.Y. Ebrahimipour, M. Mohamadi, J. Castro, N. Mollania, H. Amiri Rudbari, A. Saccá. *J. Coord. Chem.*, **68**, 632 (2015).

[53] A. Reiss, M. Mureşeanu. *J. Chil. Chem. Soc.*, **57**, 1409 (2012).

[54] A.L. Patel, M.J. Chaudhary. *J. ChemTech Res.*, **4**, 918 (2012).

[55] S. Chandra, A. Gupta. *J. Chem. Pharm. Res.*, **5**, 278 (2013).

[56] D. Nasrin, M. Ashraful Alam, M. Nazmul Hossain, M. Nazimuddin. *Chem. J.*, **3**, 13 (2013).

[57] T.E. Olalekan, D.R. Beukes, B. Van Brecht, G.M. Watkins. *J. Inorg. Chem.*, **1** (2014).

[58] I.C. Mendes, J.P. Moreira, N.L. Speziali, A.S. Mangrich, J.A. Takahashia, H. Beraldo. *J. Braz. Chem. Soc.*, **17**, 1571 (2006).

[59] B.K. Rai, R. Kumari. *Oriental J. Chem.*, **29**, 1163 (2013).

[60] M. Gülcan, M. Sönmez, I. Berber. *Turk. J. Chem.*, **36**, 189 (2012).

[61] K.Y. Djoko, M.M. Goytia, P.S. Donnelly, M.A. Schembri, W.M. Shafer, A.G. McEwan. *Antimicrob. Agents Chemother.*, **59**, 6444 (2015).

[62] A.M. Lourdes Zatón, J.P. Villamor. *Chem-Biol. Interact.*, **124**, 1 (2000).

[63] X-J. Li, K. Zheng, Y-T. Li, C-W. Yan, Z-Y. Wu, S-Y Xuan. *J. Coord. Chem.*, **68**, 928 (2015).

[64] J. Lu, J-L. Li, Q. Sun, L. Jiang, B-W. Wang, W. Gu, X. Liu, J-L. Tian, S-P. Yan. *J. Coord. Chem.*, **67**, 300 (2014).

[65] Y-J. Hu, Y. Liu, Z-B. Pi, S-S. Qu. *Bioorg. Med. Chem.*, **13**, 6609 (2005).

[66] N.M. Urquiza, M.S. Islas, S.T. Ariza, N. Jori, J.J. Martínez Medina, M.J. Lavecchia, L.L. López Tévez, L. Lezama, T. Rojo, P.A.M. Williams, E.G. Ferrer. *Chem. Biol. Interact.*, **229**, 64 (2015).

[67] E.G. Ferrer, A. Bosch, O. Yantorno, E.J. Baran. *Bioorg. Med. Chem.*, **16**, 3878 (2008).

[68] T. Sawada, K. Fukumaru, H. Sakurai. *Chem. Pharm. Bull.*, **44**, 1009 (1996).

Table 1. Analytical data, solubility, UV-vis and EPR spectroscopic data for $[Cu(PTU)_2]_2$.

Compound	$[Cu(PTU)_2]_2$
Molecular formula	$C_{28}H_{40}N_8O_4S_4Cu_2$
Analysis	
Found	C, 41.55; H, 4.92; N, 13.85; S, 15.82 %
Calcd	C, 41.64; H, 4.96; N, 13.88, S, 15.86 %
Solubility	Slightly soluble in ethanol and water. Soluble in DMSO
UV-vis spectroscopy	
Solid diffuse reflectance spectrum	λ=736 nm λ=531 nm
Solution electronic absorption spectrum	λ=808 nm (ε = 122 $M^{-1}cm^{-1}$) λ=494 nm (ε = 197 $M^{-1}cm^{-1}$)
EPR parameters	
Solid complex	$g_{\|\|}$ = 2.285, $g_{\perp}$ = 2.053, $A_{\|\|}$ = 170×10^{-4} cm^{-1}, $A_{\perp}$ = 65×10^{-4} cm^{-1}, D = 0.2650 cm^{-1}
Solution complex (DMSO solution)	$g_{\|\|}$ = 2.315 $g_{\perp}$ = 2.060, $A_{\|\|}$ = 152×10^{-4} cm^{-1}, $A_{\perp}$ = 14×10^{-4} cm^{-1}, A(2N) = 14×10^{-4} cm^{-1}.

Table 2. Assignments of some characteristic FTIR bands (cm^{-1}) of propylthiouracil (PTU) and $[Cu(PTU)_2]_2$.

PTU	$[Cu(PTU)_2]_2$ (violet)	Assignments	
3089 s	3073 w	ν(NH)	
1702 h	1702 h	ν(C=O)	
1656 s	1662 m	ν(C=C)	
1557 m	1594 s	ν(C-N) ring	
1440 m	1486 s	I	Thioamide bands
1394 w	1403 m		
1280 w	1274 s	II	
1009 w	1005 w	III	
688 w	706 m	IV	
639 w	644 m		
	419 w	ν(Cu-N)	

s = strong, m = medium, w = weak

Table 3. Minimum inhibitory concentrations (MICs) of $CuCl_2 \cdot 2H_2O$, PTU and the complex Cu-PTU for bacterial and fungal strains. MIC values in μg/mL.

	Bacterial strains				**Fungal strains**		
Compound	*E. coli* Gram (-)	*P. aeruginosa* Gram (-)	*E. faecalis* Gram (+)	*S. aureus* Gram (+)	*C. albicans*	*C. tropicalis*	*C. parapsilosis*
$CuCl_2 \cdot 2H_2O$*	375	375	375	375	>1500	>1500	>1500
PTU	>1500	>1500	>1500	>1500	>1500	>1500	1500
Cu-PTU	>375	>375	24	12	12	12	12
$[Cu(L)_2]4H_2O$**				40			40
[Cu(atsm)]***	>8			>3			
[Cu(gtsm)]***	>7			>1			
Gentamicin	0.75	1.5		0.19			
Ampicillin			0.37				
Fluconazole					>375	1.5	6

(*) Ref. [8]

(**) Data taken from Ref. [60], L = 1-amino-5-benzoyl-4-phenyl-1H-pyrimidine-2-thione.

(***) Data taken from Ref. [61] where atsm and gtsm are thiosemicarbazone derivatives.

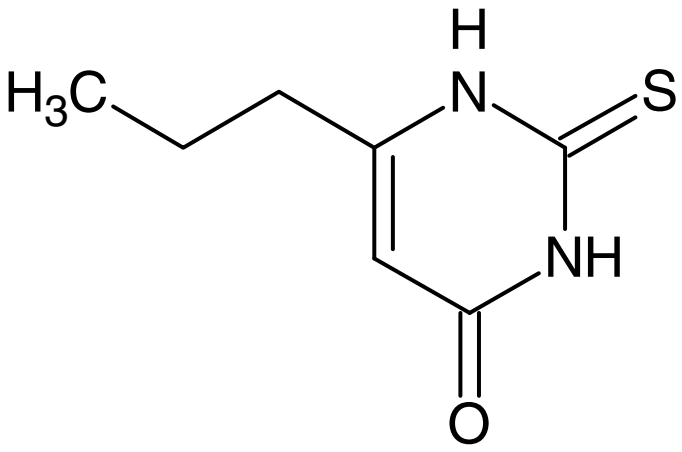

Figure 1. Formula of propylthiouracil (PTU).

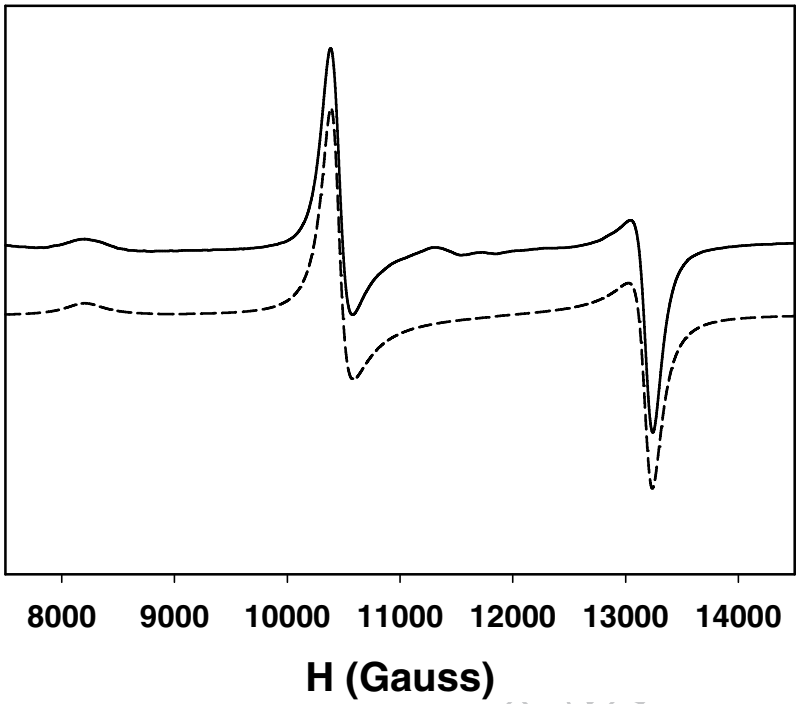

Figure 2. EPR powder spectra at 290 K (Q band, 34.1760 GHz) of $[Cu(PTU)_2]_2$ (violet) (solid line) and simulated spectrum (WINEPR SimFonia (dashed line)).

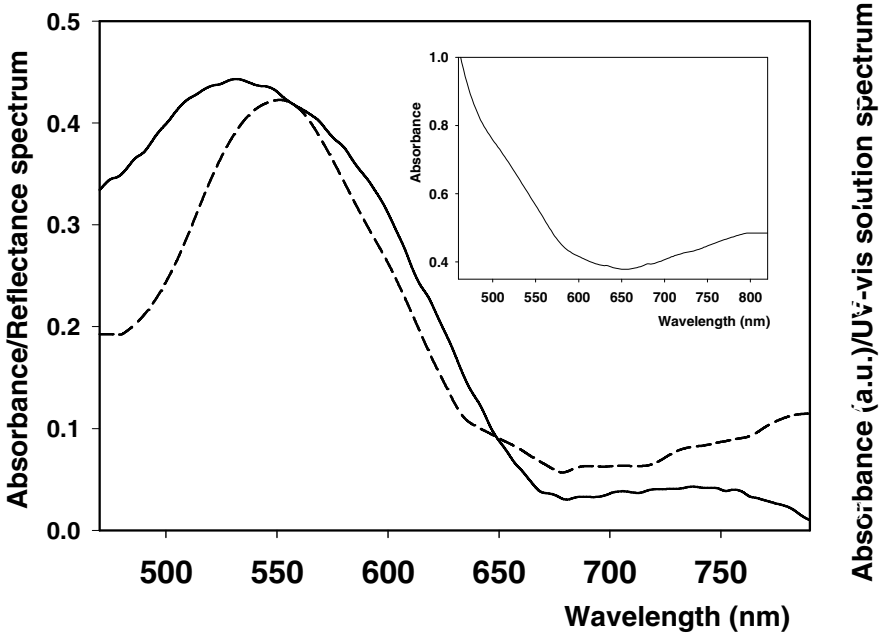

Figure 3. Solid line: diffuse reflectance spectrum of $[Cu(PTU)_2]_2$; short dashed line: UV-vis absorbance spectrum of $[Cu(PTU)_2]_2$ in ethanol (qualitative); inset: UV-vis absorbance spectrum of $[Cu(PTU)_2]_2$ in DMSO (4×10^{-3} mM either for the dimeric complex or per copper ion, 808 nm (ε = 121.5 $M^{-1}cm^{-1}$), 494 nm (ε = $M^{-1}cm^{-1}$).

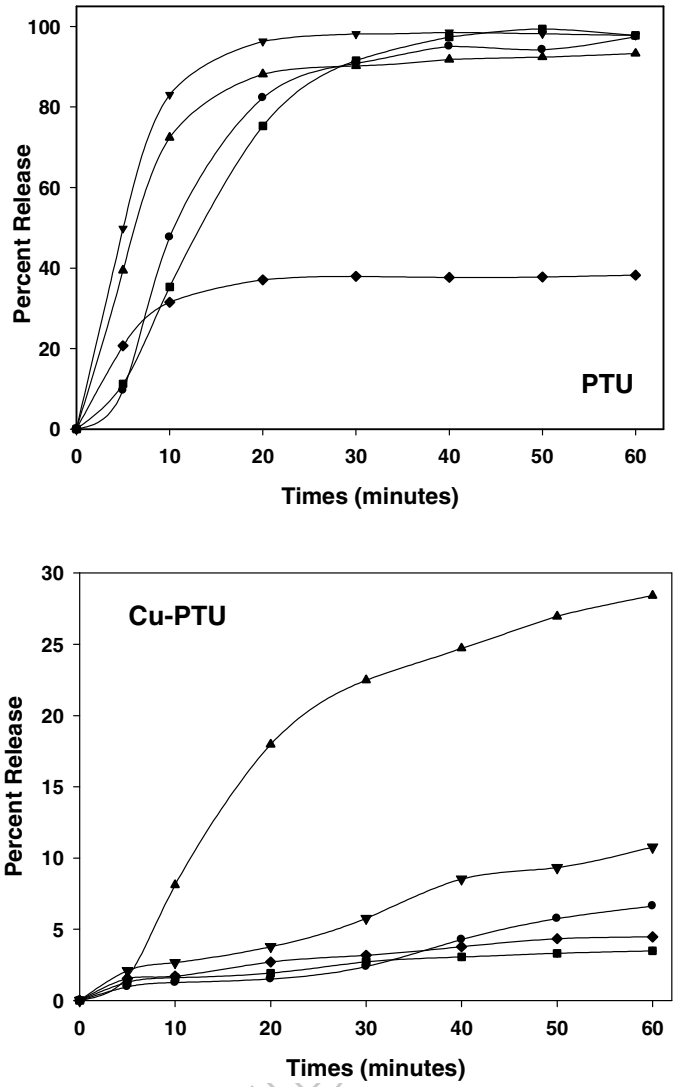

Figure 4. Dissolution profiles for PTU and $[Cu(PTU)_2]_2$ using 100 rpm (● HCl, ■ H_2O, ▲ LSNa, ♦ buffer, ▼ gastric medium).

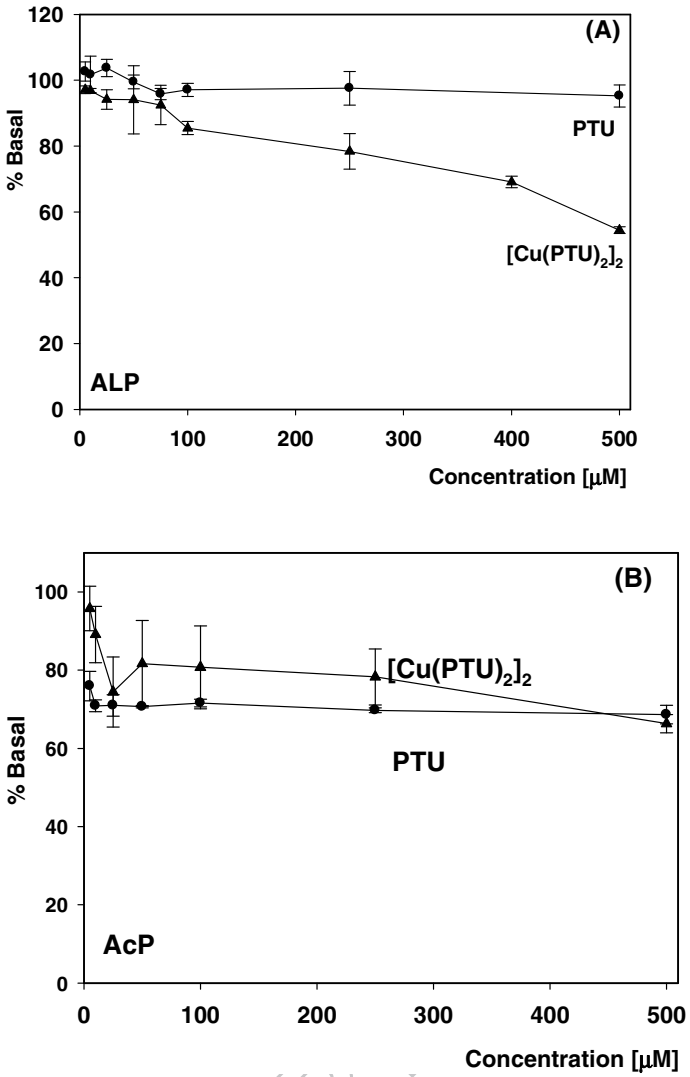

Figure 5. (A) Effect of PTU (●) and $[Cu(PTU)_2]_2$ (▲) on ALP activity from bovine intestinal mucose. Initial rate was determined by incubation of the enzyme at 37 °C for 10 min in the absence or presence of variable concentrations of the inhibitors. (B) Effect of PTU (●) and $[Cu(PTU)_2]_2$ (▲) on AcP activity. Initial rate was determined by incubation of the enzyme at 37 °C for 20 min in the absence or presence of variable concentrations of the inhibitors. The concentrations are calculated either per copper ion or for the dimeric complex. The values are expressed as the mean ± SEM of at least three independent experiments.

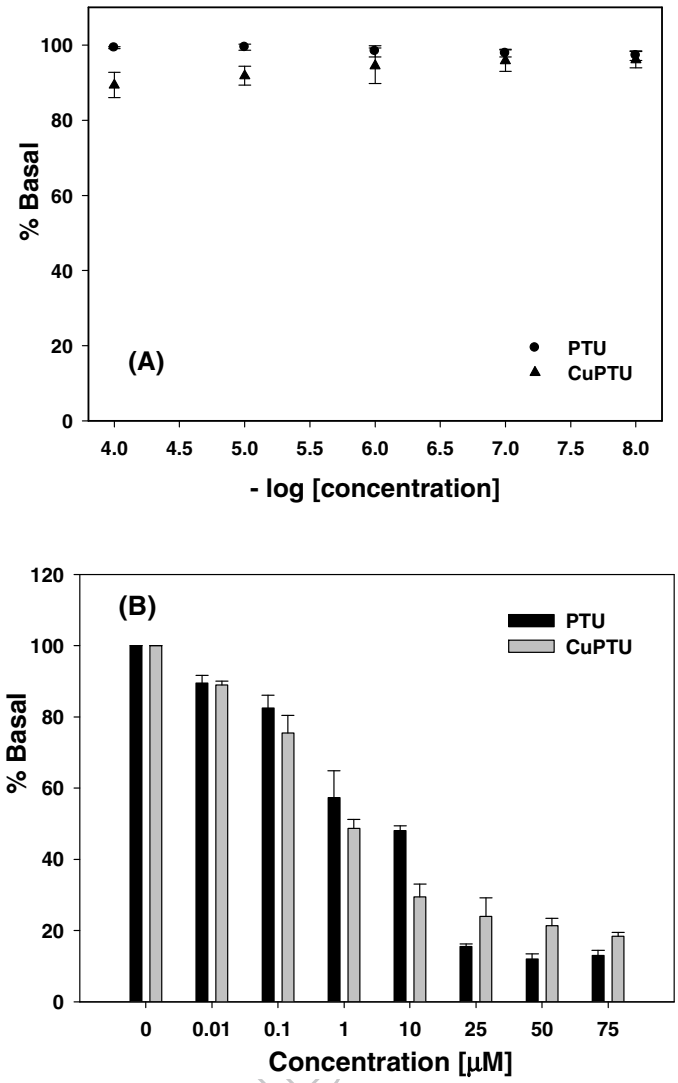

Figure 6. (A) Effects of PTU (●) and $[Cu(PTU)_2]_2$ (▲) on the reduction of nitroblue tetrazolium by nonenzymatically generated superoxide (phenazine methosulfate and reduced nicotinamide adenine dinucleotide system). (B) Effect of PTU (black bar) and $[Cu(PTU)_2]_2$ (gray bar) on the extent of deoxyribose degradation by hydroxyl radical, measured with the thiobarbituric acid method. The concentrations are calculated either per copper ion or for the dimeric complex. The values are expressed as the mean ± SEM of at least three independent experiments.

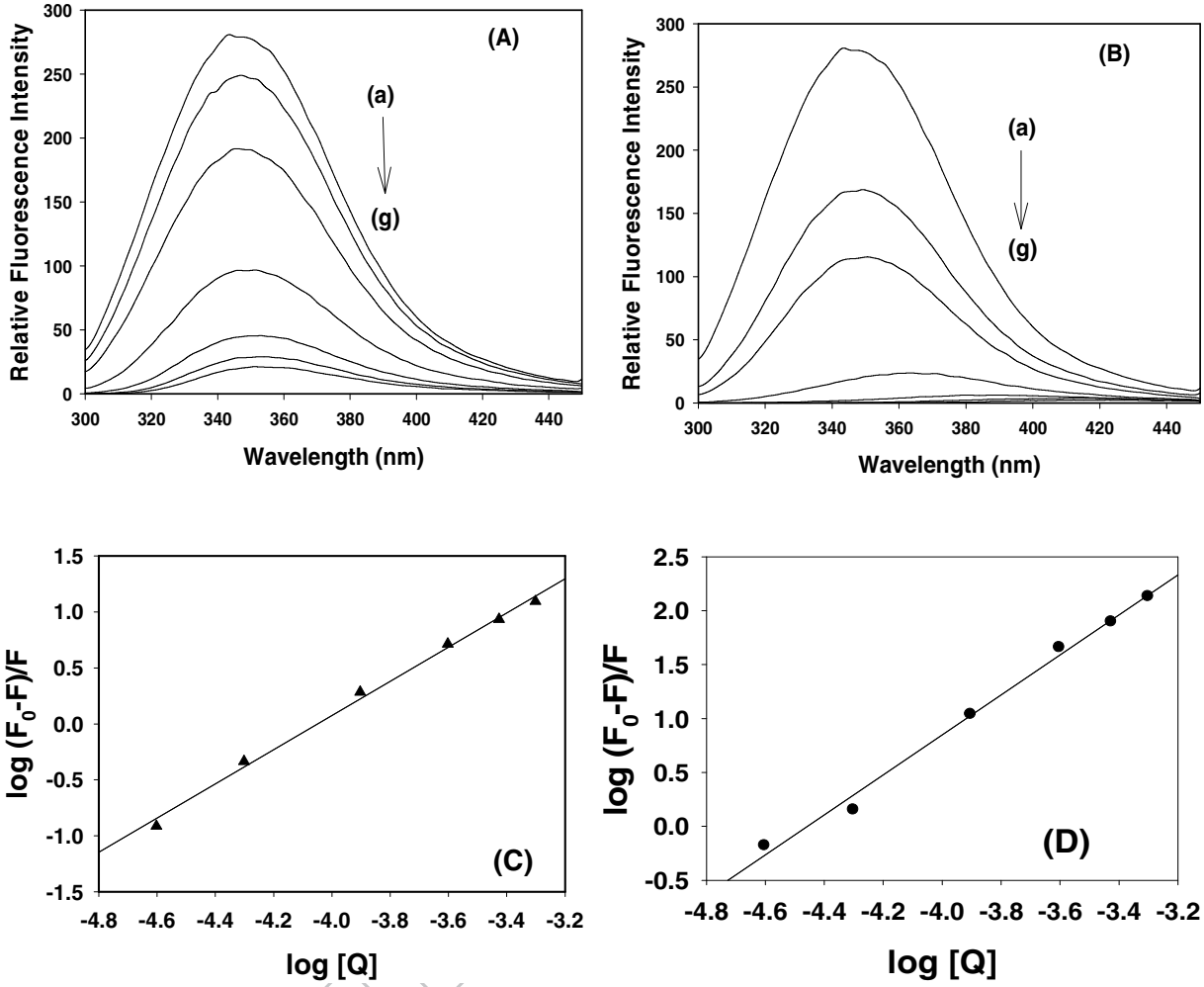

Figure 7. Fluorescence spectra of (A) PTU–BSA and (B) $[Cu(PTU)_2]_2$-BSA systems. BSA concentration was 2% w/v in all assays, and the concentrations of the additives were: (a) 0, (b) 0.25, (c) 0.50, (d) 0.75, (e) 0.125, (f) 0.250, and (g) 0.500 mM (T = 25 °C, pH 7.4, λ_{exc} = 280 nm, λ_{em} = 348 nm). Plot of log $(F_0-F)/F$ vs log [Q] for (C) PTU–BSA and (D) $[Cu(PTU)_2]_2$-BSA systems (same experimental conditions).

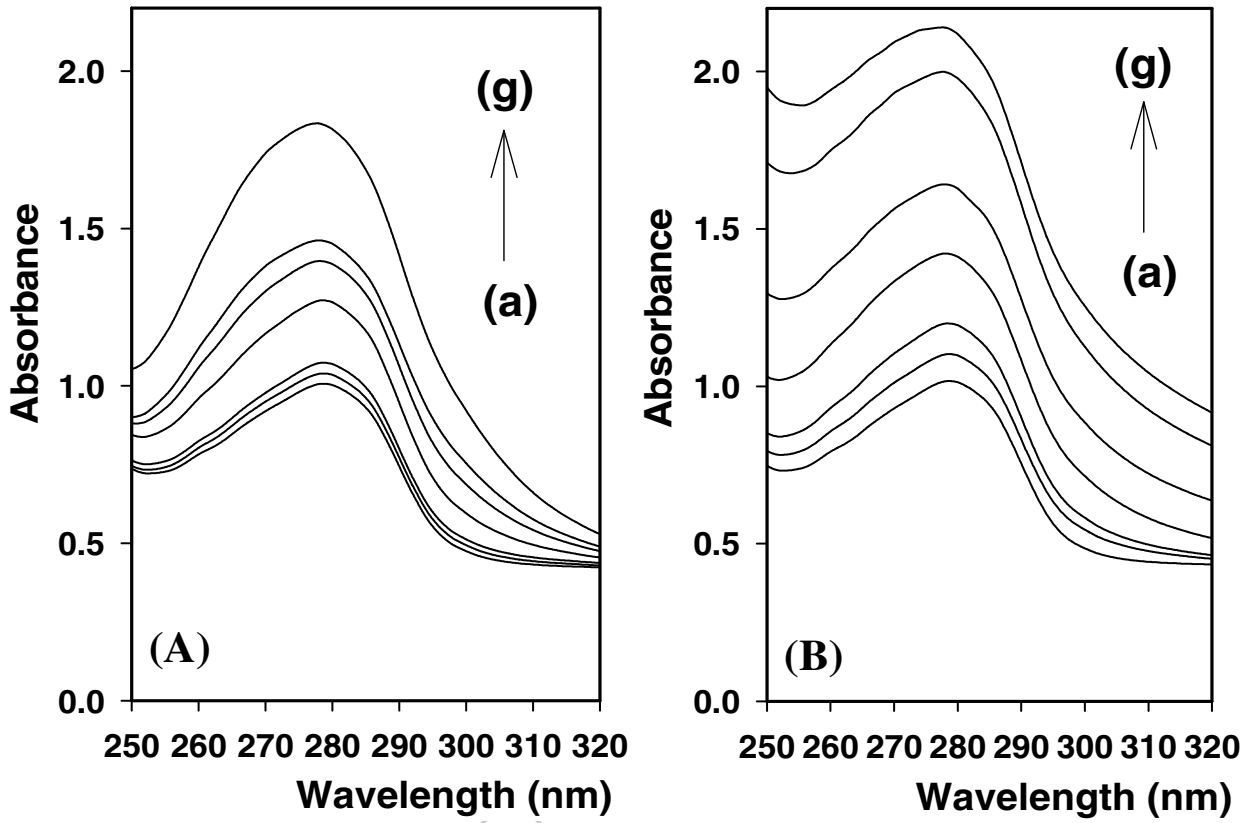

Figure 8. UV-vis spectra of (A) PTU–BSA and (B) $[Cu(PTU)_2]_2$-BSA systems. BSA concentration was 2% w/v in all assays, and the concentrations of the additives were: (a) 0, (b) 0.25, (c) 0.50, (d) 0.75, (e) 0.125, (f) 0.250, and (g) 0.500 mM (T = 25 °C, pH 7.4). The concentrations are calculated either per copper ion or for the dimeric complex.

Graphical abstract